

Capacitor current analysis of a three-level neutral point clamped converter under unbalanced loading conditions

Riyadh Toman Thahab¹, Tahani Hamodi Al-Mhana¹, Ahmed Toman Thahab²

¹Department of Electrical Engineering, College of Engineering, University of Babylon, Babylon, Iraq

²Department of Biomedical Engineering, College of Engineering, University of Babylon, Babylon, Iraq

Article Info

Article history:

Received Mar 5, 2022

Revised Jun 1, 2023

Accepted Jun 26, 2023

Keywords:

Capacitor current

Neutral point converter

Symmetrical components

Two-dimensional Fourier series

Unbalanced load

ABSTRACT

A neutral point clamped (NPC) converter is considered a forefront in industrial applications. Supplying a typically balanced stand-alone load is one of those applications. However, the loading may become unbalanced which can impact the capacitors' current and voltage ripple. In this work, an approach is proposed that analyze the capacitor current under unbalanced loading. The proposed method is based on a combination of two-dimensional Fourier series and symmetrical components. Since, two-dimensional Fourier series sectorize the spectrum into harmonics that are either defined by multiples of, fundamental, carrier or both frequencies, the method derives the Fourier coefficients for each sector, corresponding to a sequence current. Therefore, based on the presented approach, each harmonic amplitude in the spectrum sector is defined by three Fourier coefficients reflecting zero, positive and negative sequence current. The capacitor current spectrum is obtained by vector summing sequence coefficients. The method is tested on unbalanced load conditions with (out) a ground path. Results verify feasibility of the proposed method in deriving Fourier coefficients of capacitor currents that accurately reflects the loading status of the NPC. This is vital for converter design in terms of proper sizing of DC capacitor and can help in avoiding components failure.

This is an open access article under the [CC BY-SA](https://creativecommons.org/licenses/by-sa/4.0/) license.



Corresponding Author:

Riyadh Toman Thahab

Department of Electrical Engineering, College of Engineering, University of Babylon

Babylon, Iraq

Email: eng.riath.toman@uobabylon.edu.iq, riyadhtomanth.toman@wmich.edu

1. INTRODUCTION

Three-level neutral point clamped converter was first emerged for adjustable motor drive by Nabae *et al.* [1] in 1981. Compared with two level voltage source inverter (VSI), the (3L-NPC) is characterized by its high efficiency, high quality output voltage, reduced power devices voltage stress, low output current ripple and common mode voltage (CMV) steps [2]–[4]. In [5] reviewed various multi-level inverters (MLI) topologies including, neutral point clamped (also named diode clamped inverter DCI), capacitor-clamped inverter and cascaded multi-cell inverter with various control methods and applications. Based on the available literatures, the 3L-NPC is considered as the most established multi-level inverter topologies employed in various industrial applications including renewable energy systems and medium/high voltage motor drives systems [6]–[10]. In [11] showed that the three-level diode clamped inverter (DCI) is a better option to drive a brushless DC (BLDC) motor than the cascaded H-bridge inverter in terms of total harmonic distortion (THD). In addition, the 3L-NPC can drive effectively an induction motor (IM) by reducing the THD to 50% for traction application in comparison with two level inverter [12]. An improvement to low-speed response of IM driven by 3L-NPC is achieved by modifying the sensor-less

vector control approach upon using adaptive neuro-fuzzy inference system instead of proportional-integral (PI) controller in the adaptive system of a rotor flux-model reference adaptive system (RF-MRAS) [13].

The 3L-NPC converter has two capacitors connected in series to form the DC link with mid-point (neutral point N) needed for zero level in the output. The mid-point of the transistors in each leg is connected with the neutral point via clamping diodes. When the upper two switches are conducting, the output voltage is positive with a value of half Vdc. The negative output voltage of $-V_{dc}/2$ is produced when the lower two switches are conducting. However, the zero level is achieved when a combination of one upper and one lower switch is conducting [14].

To control the behavior of the 3L-NPC, various pulse-width modulation (PWM) can be used including, carrier based PWM (CB-PWM) [15]–[17], space vector modulation (SVM) [18]–[20] and selective harmonic elimination (SHE-PWM) [21]. However, the 3L-NPC inverter suffers from some drawbacks such as the imbalance of DC neutral points, the common mode voltages (CMV) and shoot through problems. One major issue of NPC topology is the balancing of DC-link capacitors. Intensive researches have been presented to maintain equal voltage across DC capacitors using various PWM techniques [14]. However, less attention has been paid to analyze the DC capacitor's current and its AC components under various operating conditions. The CB-PWM is intensively used in the industry to balance the DC-link capacitor voltage and reduce the ripple due to its simplicity [22]. Chen *et al.* [23] proposed a simple method for balancing the capacitor voltage by injecting a zero-sequence voltage determined by comparing both DC capacitor voltage with the three-phase AC voltages. A new approach using harmonic resonant controller is proposed to balance the DC capacitor voltage by controlling the position of pole and zero points with the operating airplane frequency of 400 Hz [24]. While [25] proposed a simple PWM strategy for NPC with unbalanced DC-links voltage by simplifying the conventional SVM, and taking the output voltage modulation to find a solution without depending on the position of the reference vector in the complicated space vector modulation. A combination of space vector modulation and carrier-based PWM is proposed in [26] for the 3L-NPC operating under unbalanced DC-link voltage. The selective harmonic modulation approach is also adopted for balancing the voltage of capacitors by varying the duty cycle of the switches responsible for zero-level, which depends on the output currents polarity and DC voltage, is adopted in [27]. Recently, to analyse a number of power converters and precisely derive the output voltage harmonic spectrum, two-dimensional Fourier analyses has been applied [28]. Thakur *et al.* [29] employed this approach in applications where the DC voltage input itself is polluted by harmonics, the work concluded that the DC voltage harmonics reshapes the spectrum by adding harmonics in the baseband, carrier and sidebands zones. However, all the above work has been focused on the DC capacitor voltage unbalancing issue with limited attention to the DC capacitor current despite its important role in the output voltage spectra.

For power converters design, it is very important to select the proper size of the capacitors including the DC and filter capacitor for 3L-NPC which is heavily dependent on capacitor current harmonics. Thus, an accurate analysis of capacitor current is vital. Although Orfanoudakis [30] analyzed the DC-link capacitor current for MLI using the two-dimensional Fourier series, their investigation was limited to converter operating under balanced load condition. This paper presents a detailed analysis of the DC capacitor current using two-dimensional Fourier series for 3L-NPC converter operating at conditions that involves unbalanced loading with or without the presence of a path to ground. This path will affect the flow of zero sequence current in the converter output terminals. The work presented in this paper will contribute to improving the converter design by selecting a proper capacitor size in the DC side under all operating conditions. In addition, this analysis can help in avoiding component failure due to improper selection of passive components in the DC side capacitor.

2. THE PROPOSED METHOD

Work presented in this paper considers circumstances where the three-phase load becomes unbalanced for a sustainable period of time. The latter can occur due to many reasons, such as a change in consumed power involving one or more phases of the load. Previous work presented in [30] considered capacitor current analysis of NPC converter for balanced load conditions only. A powerful tool for analyzing unbalanced conditions is the symmetrical components theory [31], [32]. According to this theory, unbalanced currents are expressed as the vector sum of zero, positive and negative sequence set of balanced phasors.

The proposed method aims to determine the Fourier coefficients for the capacitor current of the NPC converter as function of the sequence currents. The coefficients are based on the two dimensional Fourier series, that assumes two periodic variables, one for the low frequency modulating wave while the other is for the high frequency carrier of the PWM scheme [28]. The resultant spectrum produced by the two dimensional Fourier series has three sectors; baseband, carrier and sidebands sectors [28]. Hence, the proposed method must provide three spectrum coefficients for each harmonic in a sector corresponding to the zero, positive and negative sequence currents of the capacitor respectively. The resultant coefficient, which

represents current amplitude, is obtained by simply vector summing each sequence coefficient for each sector. The approach presented in this paper can be summarized in the following steps:

Step 1: Express the capacitor current in terms of timing varying sequence components.

Step 2: Develop an expression for the Fourier coefficients as function of sequence currents.

Step 3: Obtaining the resultant coefficients by combing the effects of all sequence coefficients.

Steps 2 and 3 are performed for baseband, carrier and sidebands harmonics to obtain the overall spectrum of the NPC converter capacitor current under unbalanced loads.

2.1. Capacitor current of a three-level neutral point clamped converter in terms of symmetrical components

The circuit diagram of a 3L-NPC is shown in Figure 1. Three phase load is represented by impedances, Z_a , Z_b , and Z_c . In this section, the objective is to develop an expression for capacitor current in terms of symmetrical current components. Analysis is presented for the current of upper capacitor; lower capacitor follows the same procedure [30]. The contribution of capacitor current is mathematically expressed as (1),

$$i_{C1}(t) = \sum_{x=a,b,c} i_x(t) - i_{in}(t) \quad (1)$$

where, i_x and i_{in} is the individual phase and input converter current respectively. If the input current is considered to be ripple free, hence the capacitor current is equal to the sum of all phase currents [30]. The sequence components definition in the time domain is,

$$\begin{aligned} i^0(t) &= \text{Re}(I_m^0 e^{j(\omega t + \varphi^0)}) \\ i^+(t) &= \text{Re}(I_m^+ e^{j(\omega t + \varphi^+)}) \\ i^-(t) &= \text{Re}(I_m^- e^{j(\omega t + \varphi^-)}) \end{aligned} \quad (2)$$

here $i^{0(+)(-)}(t)$, are the time domain zero, (positive) or (negative) sequence component current, $I_m^{0(+)(-)}$, is the peak value of the sequence component and $\varphi^{0(+)(-)}$, is the phase shift of the respective sequence component for a reference phase, which is usually phase a. The time domain sequence components based on the complex conjugate representation are [31],

$$\begin{aligned} i^0(t) &= \frac{1}{\sqrt{2}} (I^0 e^{j\omega t} + I^{0*} e^{-j\omega t}) \\ i^+(t) &= \frac{1}{\sqrt{2}} (I^+ e^{j\omega t} + I^{-*} e^{-j\omega t}) \\ i^-(t) &= \frac{1}{\sqrt{2}} (I^- e^{j\omega t} + I^{+*} e^{-j\omega t}) \end{aligned} \quad (3)$$

where, I^0 (I^{0*}), I^+ (I^{+*}) and I^- (I^{-*}) are the phasors of each sequence component (conjugate) at the nominal frequency. For example, $I^0 = I_m^0 e^{j\theta_0}$ and $I^{0*} = I_m^0 e^{-j\theta_0}$, other sequence phasor and conjugate are defined in a similar way. These phasors can be obtained by using the transformation matrix T [32]. Decomposing the current of phase, an into sequence component results in (4).

$$i_a(t) = i^0(t) + i^+(t) + i^-(t) \quad (4)$$

According to (3), (4) can be rewritten as (5).

$$i_a(t) = \frac{1}{\sqrt{2}} [(I^0 e^{j\omega t} + I^{0*} e^{-j\omega t}) + (I^+ e^{j\omega t} + I^{-*} e^{-j\omega t}) + (I^- e^{j\omega t} + I^{+*} e^{-j\omega t})] \quad (5)$$

Equation (5), expresses the instantaneous current of phase a as a sum of zero, positive and negative sequences. Apart the zero-sequence term, the other two sequences are expressed as the sum of the time function of the sequence itself plus the conjugate of opposite sequence. However, according to (1), capacitor current, $i_{C1}(t)$, requires expressions for, $i_b(t)$ and $i_c(t)$. These currents can be obtained by simply rotating the positive and negative sequences by, α or α^2 , while the zero sequence is identical in all phases [32]. Therefore, the AC content of the upper capacitor at the fundamental frequency and in terms of the instantaneous sequence current is expressed as (6),

$$\tilde{i}_{C1} = \underbrace{3i^o(t)}_{\text{All phases}} + \underbrace{i^+(t) + i^-(t)}_{\text{Phase a}} + \underbrace{\alpha^2 i^+(t) + \alpha i^-(t)}_{\text{Phase b}} + \underbrace{\alpha i^+(t) + \alpha^2 i^-(t)}_{\text{Phase c}} \tag{6}$$

where, \tilde{i}_{C1} is the capacitor current AC content. Here, (6) considers the AC content depicted from (1). Furthermore, each time function sequence current can be substituted by the complex conjugate representation of (3). This completes the representation of capacitor current in terms of phase sequence components.

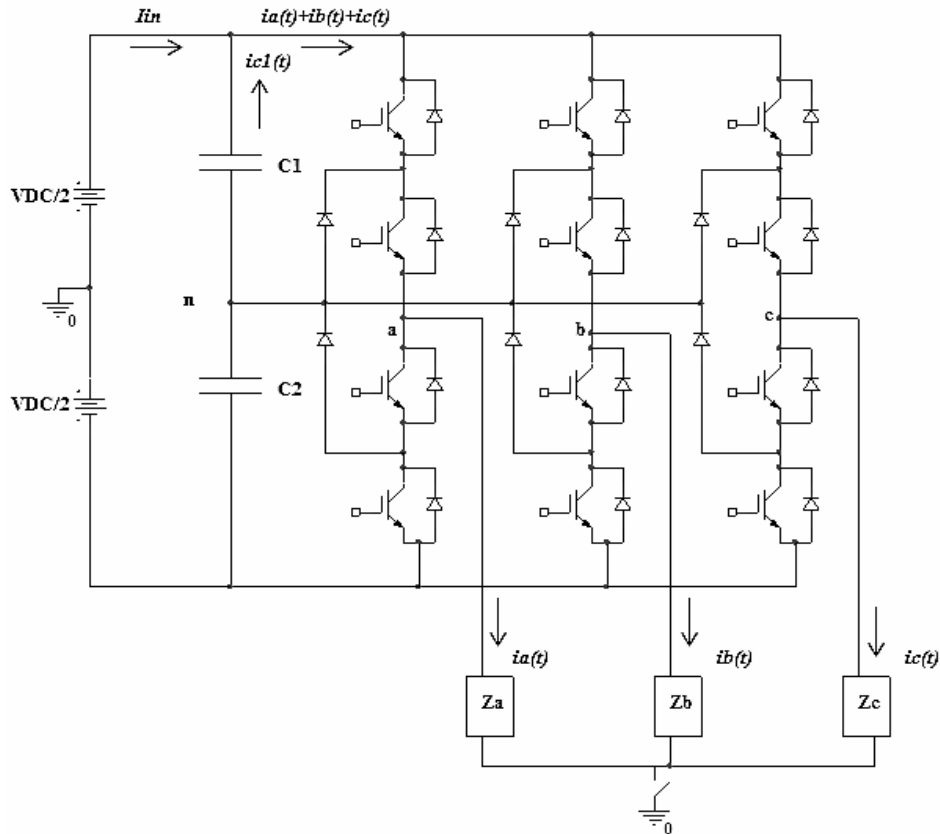


Figure 1. Three-phase three-level neutral point clamped converter with unbalanced load

2.2. Two dimensional Fourier coefficients of phase current based on symmetrical components

In this section, the aim is to derive the two-dimensional Fourier coefficients for the phase current of the 3L-NPC when supplying a non-balanced load at the output terminals. The two-dimension Fourier representation is expressed as [28],

$$f(x, y) = \frac{A_{00}}{2} + \sum_{n=1}^{\infty} (A_{on} \cos(ny) + B_{on} \sin(ny)) + \sum_{m=1}^{\infty} (A_{mo} \cos(mx) + B_{mo} \sin(mx)) + \sum_{m=1}^{\infty} \sum_{\substack{n=-\infty \\ n \neq 0}}^{\infty} (A_{mn} \cos(mx + ny) + B_{mn} \sin(mx + ny)) \tag{7}$$

where, the real/imaginary parts of the Fourier coefficients and the two periodic time variables x and y are defined as [28],

$$C_{mn} = A_{mn} + jB_{mn} = \frac{1}{2\pi^2} \int_{-\pi}^{\pi} \int_{-\pi}^{\pi} f(x, y) e^{j(mx+ny)} dx dy \tag{8}$$

$$x = \omega_c t, y = \omega_o t \tag{9}$$

here, ω_c and ω_o are the angular frequency of the carrier and low frequency modulating waveform of the PWM technique respectively. The coefficients A_{on} and B_{on} are the amplitudes of the baseband harmonics,

whereas A_{mo} and B_{mo} are amplitudes of carrier based harmonics and A_{mn} and B_{mn} are coefficients of sidebands harmonics around the carrier harmonics respectively [28].

In [28] the spectrum of the output voltage from the NPC is derived for different PWM schemes, for which $f(x,y)$ in (8) represents the various levels in the output voltage. However, in [30], this function represented the maximum current of a single converter leg, which is equal in all phase since the load considered is balanced. In this work, current is not equal in the phases of load and therefore $i_b(t)$ and $i_c(t)$ contribute to the spectrum of the capacitor current. Computation wise, it is much simpler to consider coefficients of one phase and then broaden the results to include the other two phases. In that aspect, recalling (4), phase a current is defined in terms of symmetrical components. Therefore, $f(x,y)$ for this phase is defined for each sequence component as (10),

$$f_a^o(x,y) = i^o(t), f_a^+(x,y) = i^+(t) \text{ and } f_a^-(x,y) = i^-(t) \quad (10)$$

Equation (8) is rewritten considering the definitions in (10) as (11),

$$\begin{aligned} C_{mna} = & \frac{1}{2\pi^2} \left[\int_{-\frac{\pi}{2}}^{\frac{\pi}{2}} \int_{-\pi A \cos y}^{\pi A \cos y} [f_a^o(x,y) + f_a^+(x,y) + f_a^-(x,y)] e^{j(mx+ny)} dx dy - \right. \\ & \int_{-\frac{\pi}{2}}^{\frac{\pi}{2}} \int_{-\pi}^{-\pi(1+A \cos y)} [f_a^o(x,y) + f_a^+(x,y) + f_a^-(x,y)] e^{j(mx+ny)} dx dy + \\ & \int_{-\frac{\pi}{2}}^{\frac{\pi}{2}} \int_{\pi(1+A \cos y)}^{\pi} [f_a^o(x,y) + f_a^+(x,y) + f_a^-(x,y)] e^{j(mx+ny)} dx dy \mp + \\ & \int_{\frac{\pi}{2}}^{\pi} \int_{-\pi}^{-\pi(1+A \cos y)} [f_a^o(x,y) + f_a^+(x,y) + f_a^-(x,y)] e^{j(mx+ny)} dx dy + \\ & \left. \int_{\frac{\pi}{2}}^{\pi} \int_{\pi(1+A \cos y)}^{\pi} [f_a^o(x,y) + f_a^+(x,y) + f_a^-(x,y)] e^{j(mx+ny)} dx dy \right] \quad (11) \end{aligned}$$

where, C_{mna} is the general Fourier coefficient of phase a, and A is the modulation index. Equation (11) is based on a 3L-NPC with natural sampling PD-PWM scheme where the integral limits defines the boundaries where $f(x,y)$ is constant [28]. Voltage wise, there are three zones on the x, y contour, which corresponds to, V_{DC} , 0 and $-V_{DC}$, where $f(x,y)$ is constant as illustrated in [28]. However, since the function represents a current, then the zone which reflects a current flow from the converter side to the load is considered only [30]. Hence, with respect to (11), only the first term is considered and is rewritten based on (5) and (10) to yield a general Fourier coefficient of,

$$\begin{aligned} C_{mna} = & \frac{1}{2\sqrt{2}\pi^2} \left[\int_{-\frac{\pi}{2}}^{\frac{\pi}{2}} \int_{-\pi A \cos y}^{\pi A \cos y} (I^o e^{jy} + I^{o*} e^{-jy}) e^{j(mx+ny)} dx dy + \int_{\frac{\pi}{2}}^{\pi} \int_{-\pi A \cos y}^{\pi A \cos y} (I^+ e^{jy} + \right. \\ & \left. I^{-*} e^{-jy}) e^{j(mx+ny)} dx dy + \int_{-\frac{\pi}{2}}^{\frac{\pi}{2}} \int_{-\pi A \cos y}^{\pi A \cos y} (I^- e^{jy} + I^{+*} e^{-jy}) e^{j(mx+ny)} dx dy \right] \quad (12) \end{aligned}$$

According to (12), the Fourier coefficient, C_{mna} has a contribution from zero, positive and negative sequence currents. These are denoted as, C_{mna}^o, C_{mna}^+ , and C_{mna}^- respectively. Furthermore, apart from the zero sequence, these sequence coefficients are not explicit since the positive and negative components appear as complex conjugates. The zero sequence Fourier coefficients derivations are shown below for baseband, carrier and sideband harmonics. Formulas for positive and negative coefficients are provided without derivation since they follow a similar procedure. The coefficient, C_{mna}^o , with $n=0$ and $m=0$ is,

$$C_{00a}^o = \frac{1}{2\sqrt{2}\pi^2} \int_{-\frac{\pi}{2}}^{\frac{\pi}{2}} [2I^o \pi A \cos(y) e^{jy} + 2I^{o*} \pi A \cos(y) e^{-jy}] dy = \frac{A}{2\sqrt{2}} (I^o + I^{o*}) \quad (13)$$

Equation (13) provides the average Fourier coefficient for the zero-sequence current which is equal to that of phase b and c. The harmonic content due to the carrier only, $n=0$ and $m=1, 2, 3, 4, \dots$

$$C_{m0a}^o = \frac{1}{\sqrt{2}\pi^2 m} \int_{-\frac{\pi}{2}}^{\frac{\pi}{2}} [I^o e^{jy} \sin(\pi A m \cos(y)) + I^{o*} e^{-jy} \sin(\pi A m \cos(y))] dy \quad (14)$$

Equation (14) shows a sine function with a cosine function argument in both zero-sequence phasor and its complement. This function is expressed as (15).

$$\sin(\pi A m \cos(y)) = \text{Imag} (e^{j\pi A m \cos(y)}) \quad (15)$$

This exponent can be expanded into a Bessel series defined as [28], [33],

$$Imag(e^{j\pi Am \cos(y)}) = 2 \sum_{k=0}^{\infty} (-1)^k J_{2k+1}(\pi Am) \cos(2k + 1)y \tag{16}$$

where $J(\pi Am)_{2k+1}$: is the Bessel function of order $2k+1$. Substitution of (16) into (14) gives,

$$C_{m0a}^o = \frac{2}{\sqrt{2\pi^2 m}} \int_{-\frac{\pi}{2}}^{\frac{\pi}{2}} [I^o e^{jy} \sum_{k=0}^{\infty} (-1)^k J_{2k+1}(\pi Am) \cos(2k + 1)y + I^{o*} e^{-jy} \sum_{k=0}^{\infty} (-1)^k J_{2k+1}(\pi Am) \cos(2k + 1)y] dy \tag{17}$$

The integral in (17) has a non-zero value only at $k=0$. Therefore, C_{m0a}^o , is given by (18),

$$C_{m0a}^o = \frac{-1}{\sqrt{2\pi m}} [I^o J_1(\pi Am) + I^{o*} J_1(\pi Am)] \tag{18}$$

Content from baseband harmonics with $m = 0$ and $n \neq 0$,

$$C_{0na}^o = \frac{A}{\sqrt{2\pi}} \int_{-\frac{\pi}{2}}^{\frac{\pi}{2}} [I^o e^{j(n+1)y} \cos(y) + I^{o*} e^{j(n-1)y} \cos(y)] dy \tag{19}$$

Which yields a compact form of,

$$C_{0na}^o = \frac{2A}{\sqrt{2\pi}} \left[\frac{I^o (\cos(\frac{\pi n}{2}) - j \sin(\frac{\pi n}{2})) (\sin(\pi n) - j \cos(\pi n) + j)}{n(n+2)} + \frac{I^{o*} (\cos(\frac{\pi n}{2}) - j \sin(\frac{\pi n}{2})) (\sin(\pi n) - j \cos(\pi n) + j)}{n(n-2)} \right] \tag{20}$$

The content from sidebands harmonic with $m=1, 2, 3$ and $n \neq 0$, but n is either odd or even,

$$C_{mna}^o = \frac{1}{2\sqrt{2\pi^2}} \left[\int_{-\frac{\pi}{2}}^{\frac{\pi}{2}} \int_{-\pi A \cos y}^{\pi A \cos y} (I^o e^{jy(n+1)} e^{jmx} + I^{o*} e^{jy(n-1)} e^{jmx}) dx dy \right] \tag{21}$$

Performing the first integration yields and substituting (16) gives,

$$C_{mna}^o = \frac{2}{\sqrt{2\pi^2 m}} \int_{-\frac{\pi}{2}}^{\frac{\pi}{2}} [I^o e^{jy(n+1)} \sum_{k=0}^{\infty} (-1)^k J_{2k+1}(\pi Am) \cos(2k + 1)y + I^{o*} e^{jy(n-1)} \sum_{k=0}^{\infty} (-1)^k J_{2k+1}(\pi Am) \cos(2k + 1)y] dy \tag{22}$$

Carrying out the final integration, the zero-sequence side band Fourier coefficients is expressed as (23),

$$C_{mna}^o = \frac{2}{\sqrt{2\pi^2 m}} \sum_{k=0}^{\infty} (-1)^k J_{2k+1}(\pi Am) \left\{ I^o \left[\frac{-(2\cos(\pi k)T_1 - 2T_2 \sin(\pi k) + 4kT_1 \cos(\pi k) - 2nT_2 \sin(\pi k))}{(4k^2 + 4k - n^2 - 2n)} \right] + I^{o*} \left[\frac{(2\cos(\pi k)T_1 + 2T_2 \sin(\pi k) + 4kT_1 \cos(\pi k) - 2nT_2 \sin(\pi k))}{(4k^2 + 4k - n^2 + 2n)} \right] \right\} \tag{23}$$

where, $T_1 = \sin(\pi n/2)$ and $T_2 = \cos(\pi n/2)$.

Equation (23) is valid for odd and even values of n . Therefore, C_{mna}^o , represents the current amplitude of a sideband harmonic due to the flow of zero sequence current. Sideband orders that result in infinite amplitudes for certain values of k , are treated by considering the limit for the zero sequence and conjugate terms. Finally, the Fourier coefficients corresponding to positive and negative sequence currents components are shown below for carrier, baseband and sidebands. Equations (24)-(26) are extension of expressions in (18), (20) and (23) but they reflect contribution from positive and negative sequence currents.

$$C_{m0a}^{+(-)} = \frac{-1}{\sqrt{2\pi m}} [I^{+(-)} J_1(\pi Am) + I^{-(+)*} J_1(\pi Am)] \tag{24}$$

$$C_{0na}^{+(-)} = \frac{2\pi A}{\sqrt{2\pi^2}} \left[\frac{I^{+(-)} (\cos(\frac{\pi n}{2}) - j \sin(\frac{\pi n}{2})) (\sin(\pi n) - j \cos(\pi n) + j)}{n(n+2)} + \frac{I^{-(+)*} (\cos(\frac{\pi n}{2}) - j \sin(\frac{\pi n}{2})) (\sin(\pi n) - j \cos(\pi n) + j)}{n(n-2)} \right] \tag{25}$$

$$C_{mna}^{+(-)} = \frac{2}{\sqrt{2\pi^2 m}} \sum_{k=0}^{\infty} (-1)^k J_{2k+1}(\pi Am) \left\{ I^{+(-)} \left[\frac{-(2\cos(\pi k)T_1 - 2T_2 \sin(\pi k) + 4kT_1 \cos(\pi k) - 2nT_2 \sin(\pi k))}{(4k^2 + 4k - n^2 - 2n)} \right] + I^{-(+)*} \left[\frac{(2\cos(\pi k)T_1 + 2T_2 \sin(\pi k) + 4kT_1 \cos(\pi k) - 2nT_2 \sin(\pi k))}{(4k^2 + 4k - n^2 + 2n)} \right] \right\} \quad (26)$$

Equations (18), (20), (23), (24), (25) and (26) express Fourier coefficients corresponding to each sequence for phase a current. Fourier coefficients for the remaining two phases involves only shifting the coefficients of positive and negative sequences by α or α^2 (at fundamental frequency) with the zero sequence coefficients remaining the same in all phases.

2.3. Determination of capacitor current spectrum/resultant coefficients

The coefficients determined in the preceding section represent the amplitudes of the spectrum for each sector in phase a current. To proceed to the capacitor current spectrum, it is necessary to obtain the resultant coefficients for every sector of the spectrum. The latter can be determined with reference to (6), for example since, total zero sequence in the capacitor current is three times that of the reference phase, then the zero-sequence coefficient is also three times that of reference phase a. Positive and negative sequence coefficients of the capacitor current spectrum can be obtained in terms of the reference phase coefficients. If C_{mn} defines the resultant Fourier coefficient of a sector, then this coefficient is expressed as (27),

$$C_{mn} = C_{mna}^o + C_{mna}^+ + C_{mna}^- + C_{mnb}^o + C_{mnb}^+ + C_{mnb}^- + C_{mnc}^o + C_{mnc}^+ + C_{mnc}^- \quad (27)$$

Coefficients of phase b and c are α shifted versions of their counterparts for phase a, hence for n order of the nominal frequency, C_{mn} can be written as (28),

$$C_{mn} = 3C_{mna}^o + C_{mna}^+ + C_{mna}^- + \alpha^{2n}C_{mna}^+ + \alpha^n C_{mna}^- + \alpha^n C_{mna}^+ + \alpha^{2n}C_{mna}^- \quad (28)$$

Regrouping terms in (28) results in,

$$C_{mn} = 3C_{mna}^o + (1 + \alpha^n + \alpha^{2n})C_{mna}^+ + (1 + \alpha^n + \alpha^{2n})C_{mna}^- \quad (29)$$

Equation (29) provides the capacitor current amplitudes for a general sector of the spectrum. When determining amplitudes of the baseband harmonics (or baseband sector), the coefficient of (29) become, C_{0n} . If the carrier harmonics are required, the coefficient is, C_{m0} . For the sideband harmonics left and right of the carrier harmonic, the coefficient is naturally, C_{mn} .

3. RESULTS AND DISCUSSION

In this section, simulations are carried out for the NPC converter under different load conditions. The cases considered are balanced, unbalanced grounded and unbalanced ungrounded loads. The main aim is to study the frequency content in the capacitor current corresponding to each of the loading condition mentioned above. This frequency content involves determination of the two dimensions Fourier coefficients based on the proposed method. The converter is controlled through a phase disposition pulse width modulation (PD-PWM) scheme with an output phase voltage level of $-V_{DC}$, 0, and V_{DC} [28]. Parameters for the simulations are given in Table 1. The NPC converter is simulated in MATLAB/Simulink platform which is shown in Figure 2.

Table 1. Parameters of simulations

Parameter	Value
Main DC voltage input, V_{DC}	400 V
Fundamental value of output AC voltage	360 V
Converter capacitors, C1, C2	1 mF [30]
ESR for capacitor	0.5 Ω
Balanced load RMS current, phase shift	63.63 A, $\theta = -30^\circ$
Unbalanced load RMS currents, phase shift	$I_a = 63.63$ A, $\theta_a = -30^\circ$ $I_b = 106$ A, $\theta_b = -60^\circ$ $I_c = 14.14$ A, $\theta_c = -20^\circ$
Nominal frequency of converter output voltage	$f = 60$ Hz
Amplitude modulation index	A=0.9
Frequency modulation index	$m_f = 100$

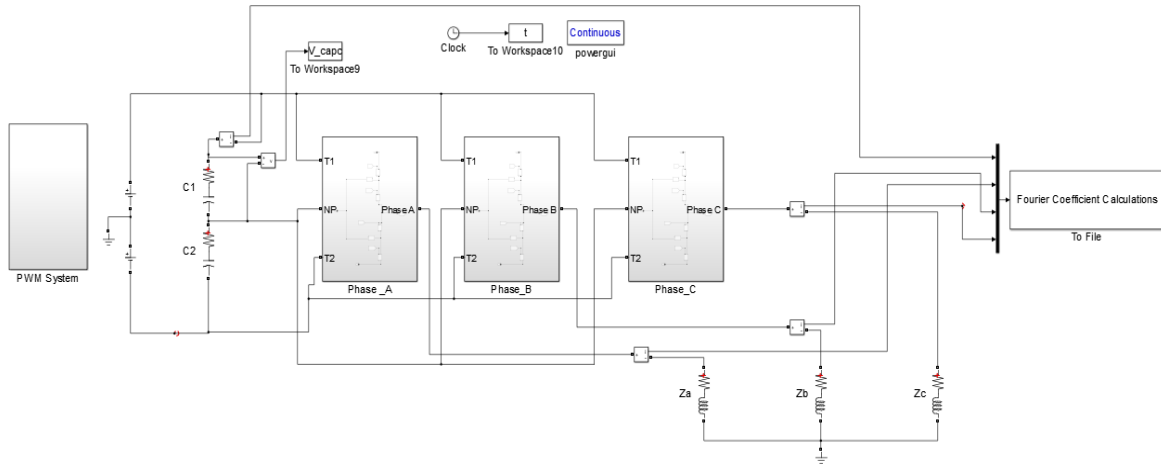


Figure 2. Simulation setup

3.1. Frequency content of capacitor current for balanced grounded load

In this case the load is balanced, output voltage (phase and line to line), load current, capacitor current and voltage are shown in Figures 3(a), 3(b), 3(c), and 3(d) respectively. Here, the capacitor current shows a non-sinusoidal behavior due to the harmonic content, which is analyzed by the two-dimensional Fourier series. Zero sequence current is equal to zero and hence the coefficient, C_{mna}^0 has very small value. This small value is attributed to the imbalances caused by the neutral point of the converter capacitors. Spectrum of sequence currents (for reference phase a) is shown in Figures 4(a) to 4(i), which is represented by, C_{mna}^0 , C_{mna}^+ , and C_{mna}^- . Although, no negative sequence current exists in this case, however, C_{mna}^- has values for all spectrum sectors as shown in Figures 4(d), 4(e) and 4(f). This is attributed to the conjugate of positive sequence current, I^{+*} for different cases of n and m , as defined by (24) to (26). At the phase level, it is reported that in the baseband sector, a 60 HZ component is present, other harmonics are odd multiples of the fundamental frequency and no even multiples exist at this sector of the spectrum. At the carrier sector, with $m=1$, a singular harmonic exists, defined by the coefficients, C_{10a}^+ & C_{10a}^- and for $m=2$, harmonics are defined by coefficients, C_{20a}^+ & C_{20a}^- . Here, the coefficients for positive and negative sequence are equal in magnitude. This can be verified by revisiting (24), where the positive sequence coefficient is, $C_{m0a}^+ = \frac{-1}{\sqrt{2\pi m}} [I^+ J_1(\pi Am) + I^{-*} J_1(\pi Am)]$, the second term is zero since no negative sequence current exists (the load being balanced). As for the negative sequence coefficient, $C_{m0a}^- = \frac{-1}{\sqrt{2\pi m}} [I^- J_1(\pi Am) + I^{+*} J_1(\pi Am)]$, here the first term is zero, hence the magnitude of the carrier harmonic coefficient is the same for each sequence. Odd and even side bands exist around the carrier harmonics reflected by the coefficients, C_{mna}^+ and C_{mna}^- at $m=1, 2$.

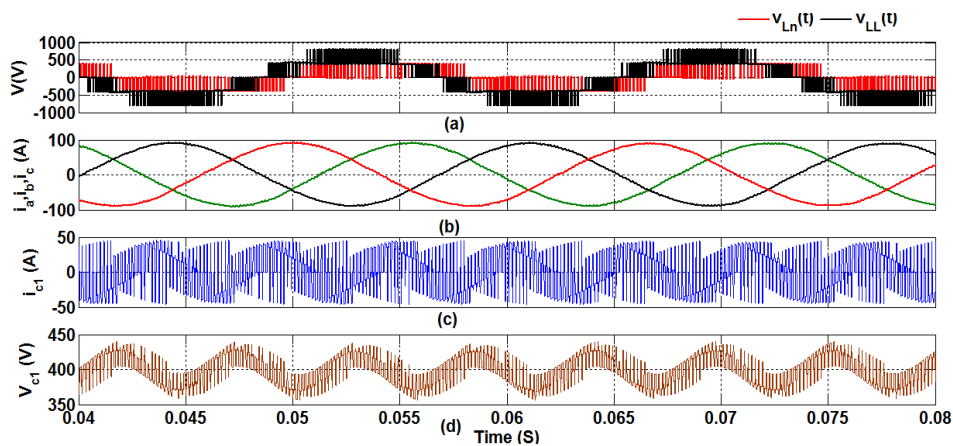


Figure 3. NPC voltages and currents for balanced load, (a) phase and line-line output voltage, (b) load currents, (c) upper capacitor current, and (d) capacitor voltage

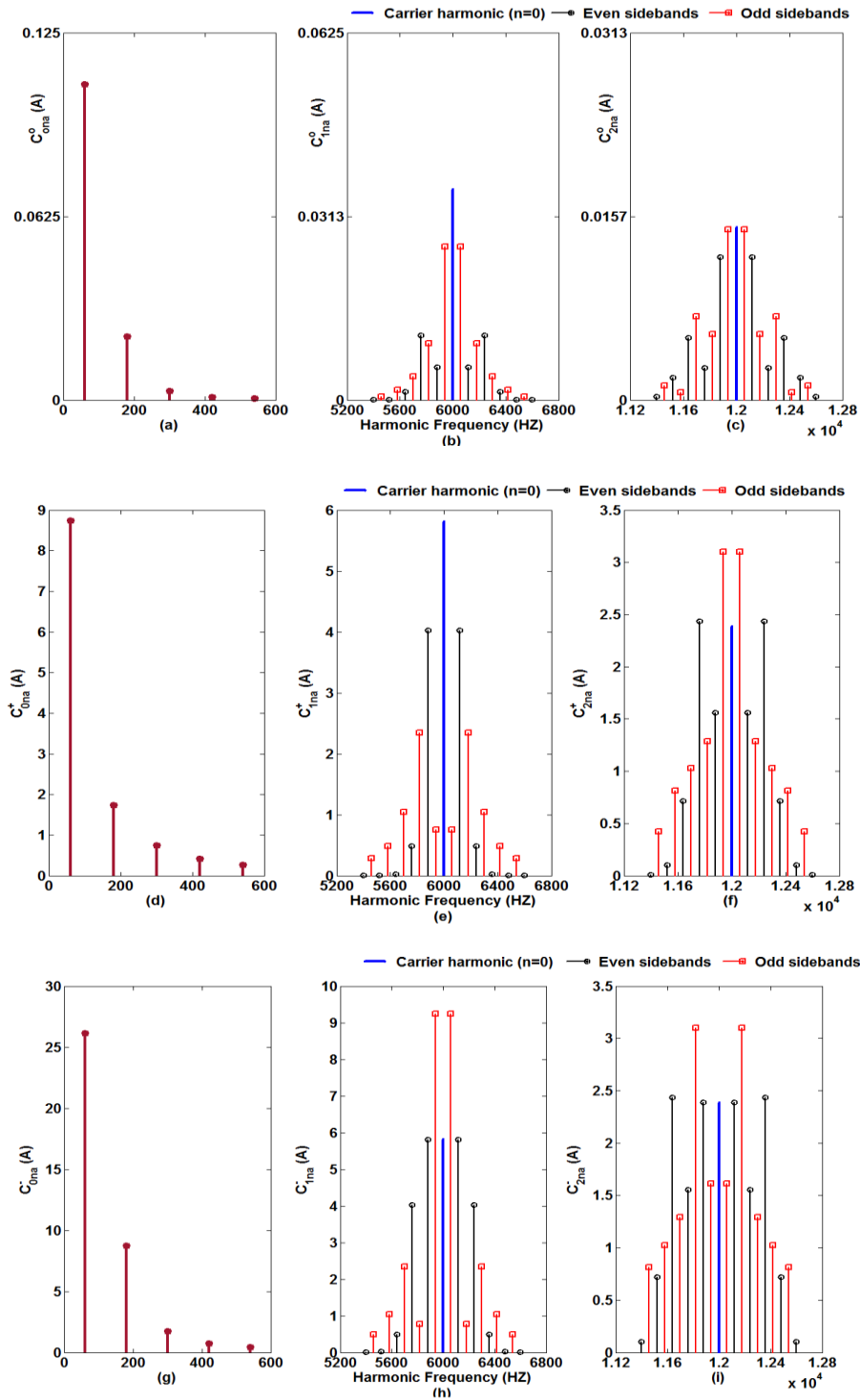


Figure 4. Spectrum per sequence current of phase a for balanced load, (a) baseband sector for zero sequence, (b) carrier and sidebands sector for zero sequence, $m=1$, (c) carrier and sidebands sector for zero sequence, $m=2$, (d) baseband sector for positive sequence, (e) carrier and sidebands sector for positive sequence, $m=1$, (f) carrier and sidebands sector for positive sequence, $m=2$, (g) baseband sector for negative sequence, (h) carrier and sidebands sector for negative sequence, $m=1$, and (i) carrier and sidebands sector for negative sequence, $m=2$

The capacitor current spectrum per sector is shown in Figure 5. If the baseband sector is considered, with reference to Figure 5(a), amplitudes are marked by either i or ii. For the first amplitude i, this represents

current amplitude at the fundamental frequency. What is interesting is that although this low frequency amplitude exists at the phase level, it is nearly diminished in the capacitor current. This can be verified by considering (29). At this amplitude, where, $n=1$, $(1 + \alpha^n + \alpha^{2n}) = 0$, hence positive and negative sequence coefficients of (29) are nullified, resulting in, $C_{01} = 3C_{01a}^o$, where C_{01a}^o is very small for all sectors of the spectrum as depicted in Figures 4(a) to 4(c). As for second and third amplitudes denoted by i, these are zero, since they correspond to harmonics with $n = 5.7$ where the value of the above identity for α is null. This means, $C_{05} = C_{07} = 0$. Coefficients in the baseband marked with ii, are those associated with harmonics of orders, $n = 3.9$. Here, the identity, $(1 + \alpha^n + \alpha^{2n}) = 3$ and hence coefficients for these orders are equal to, $C_{03} = 3C_{03a}^+ + 3C_{03a}^-$ and $C_{09} = 3C_{09a}^+ + 3C_{09a}^-$ (zero coefficient is nearly zero).

For the carrier sector, defined by coefficient, C_{10} , and C_{20} shown in Figures 5(b) and 5(c) respectively, these coefficients are evaluated by (29), by setting, $n=0$. This yields, $(1 + \alpha^n + \alpha^{2n}) = 3$. Hence, $C_{10} = 3C_{10a}^+ + 3C_{10a}^-$ and, $C_{20} = 3C_{20a}^+ + 3C_{20a}^-$. The sidebands around the carrier harmonic are classified as odd or even depending on the value of n . In addition, the value n determines whether a sideband exist or not. Reference to Figure 5(b), the first odd sideband, defined by the coefficient, C_{11} , with a frequency of, $f = m * (m_f \times f) \pm n * f = 5,940$ HZ and $6,060$ HZ, is zero since, for $n=1$ the identity, $(1 + \alpha^n + \alpha^{2n}) = 0$. Only at $n=3$, an odd sideband attains a non-zero value. This sideband has a coefficient given by, $C_{13} = 3C_{13a}^+ + 3C_{13a}^-$. Other odd sideband with non-zero value is at, $n=9$. For even sidebands, at, $n = 2.4$ which corresponds to frequencies of, $6,000 \pm 120$ HZ and $6,000 \pm 240$ HZ, the identity, $(1 + \alpha^n + \alpha^{2n}) = 0$ and hence, $C_{12} = C_{14} = 0$. The first even sideband appears at $n = 6$, where $(1 + \alpha^n + \alpha^{2n}) = 3$ and hence the coefficient is given by, $C_{16} = 3C_{16a}^+ + 3C_{16a}^-$. Other even sidebands are zero.

It is worth mentioning here, that above discussion also holds for, $m=2$ as far as the order of the odd and even sidebands are concerned. However, the value of the coefficients differs from the, $m=1$, sector since the amplitudes depend on the value of m . The analysis in this section reveals the same result as these reported in [30] and will serve as a reference when considering unbalanced loading in the following sections.

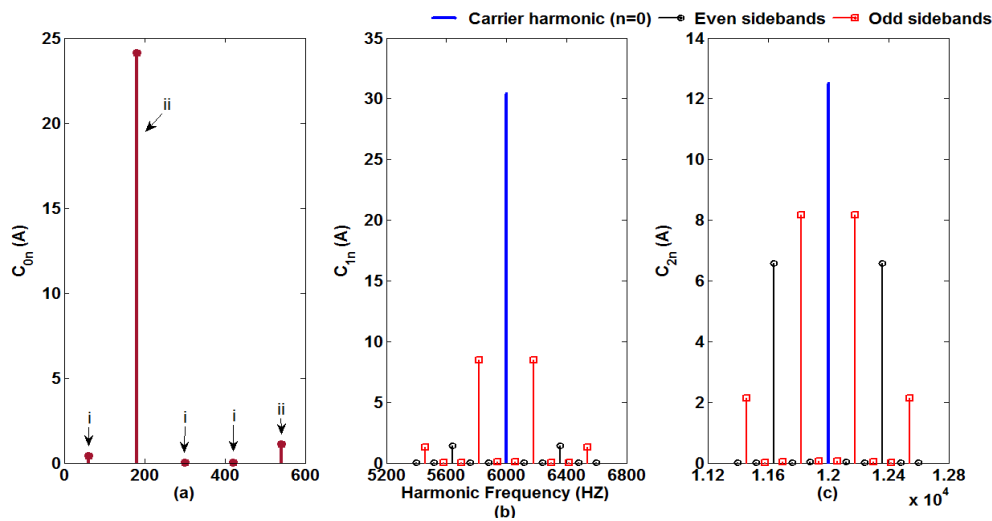


Figure 5. Spectrum of capacitor current based on combined sequence spectrum for balanced load, (a) base band, (b) carrier and sidebands at $m=1$, and (c) carrier and sidebands at $m=2$

3.2. Frequency content of capacitor current for unbalanced grounded load

This part of the simulation considers the case of unbalanced load with a ground path. Figures 6(a) to 6(d) represents the output voltage, current, capacitor current and voltage respectively for this load condition. In this scenario, negative and zero sequence currents exist and will contribute to all Fourier coefficients in the different sectors of the spectrum. For the zero sequence coefficients at the baseband sector of phase a current, harmonics have identical positions; however, amplitudes are very high compared to the balanced load scenario, as shown in Figure 7(a). This also holds for the carrier and sideband harmonics at, $m = 1$ and 2 , which are shown in Figures 7(b) and 7(c) respectively. Furthermore, the baseband sector, corresponding to positive sequence current, contains harmonic amplitudes that are significantly larger than those of the balanced load case, especially for low order harmonics as shown in Figure 7(d). For example, phase a current has, 60 Hz, amplitude of approximately 24.9 A compared to only 8.8 A for the balanced load case. This increase is due to the conjugate current of the negative sequence, I^{-*} , which exists due to

the unbalanced nature of the load. Other sectors of the spectrum exhibit a similar increase as depicted in Figures 7(e) and 7(f). Fourier coefficients corresponding to the negative sequence current, for each spectrum sector, are shown in Figures 7(g) to 7(i). For this case, the amplitudes also show an increase compared to that of the balanced case.

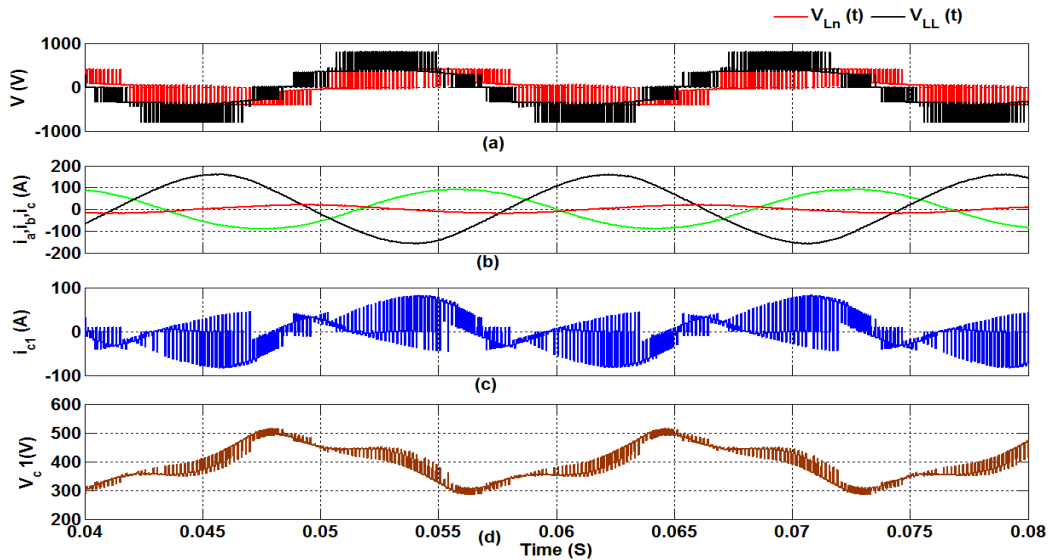


Figure 6. NPC voltages and currents for unbalanced/grounded load, (a) phase and line-line output voltage, (b) load currents, (c) upper capacitor current, and (d) capacitor voltage

The capacitor current spectrum for this type of loading is shown in Figures 8(a) to 8(c) for all sectors. The coefficient, C_{01} (first amplitude marked with i), which represent a 60 HZ amplitude, has very high value, approximately 34.8 A when compared to approximately zero in the balanced case. This can be explained with reference to (29), where, $(1 + \alpha^n + \alpha^{2n})C_{01a}^+ = (1 + \alpha^n + \alpha^{2n})C_{01a}^- = 0$, resulting in, $C_{01} = 3C_{01a}^0$. And since the zero sequence coefficients are heavily present in this type of loading, the fundamental frequency amplitude appears with a high amplitude in the capacitor spectrum, this analysis also holds for other amplitude marked as i in Figure 8(a). These amplitudes, specially, C_{01} , will significantly affect the capacitor current and resulting voltage ripple in the capacitor of the NPC converter. It is worth mentioning here, that; C_{03} and C_{09} , amplitudes that are marked with ii in Figure 8(a), undergo minor value change compared to that of the balanced case. Carrier sector, with, $m = 1$ and $n = 0$, shown in Figure 8(b), which is, $C_{10} = 3C_{10a}^0 + 3C_{10a}^+ + 3C_{10a}^-$, yet this coefficient undergoes minor value changes when comparing it with the corresponding coefficient for the balanced case. It is interesting to note that the sidebands sector is packed with harmonics that were zero in the balanced case.

These are depicted in Figures 8(b) and 8(c) for $m=1$ and 2 respectively. As an example, amplitude, C_{11} , is zero in the balanced load case, but for unbalanced grounded load, $C_{11} \approx 4$ A. This is due to the presence of the zero-sequence component in each of the phase current, hence, $C_{11} = 3C_{11a}^0$. Even sidebands at, $n = 2, 4$, have also zero amplitudes in balanced case, but now have values again due to the zero-sequence coefficient of each phase. Therefore, $C_{12} = 3C_{12a}^0$ and $C_{14} = 3C_{14a}^0$. The forgoing discussions are also held for carrier and sidebands sector for the case of, $m=2$. The analysis clearly indicates that the capacitor current will accommodate several harmonics. These will in turn significantly affect the rms value of this current.

3.3. Frequency content of capacitor current for unbalanced ungrounded load

For this part, a three-wire unbalanced load is considered. Since the neutral wire does not exist, no zero sequence current flows [32]. Therefore, the spectrum of the capacitor current is restructured compared to that of section 3.2 above. The outputs of the converter and capacitor voltage and current are shown in Figures 9(a) to 9(d). Although zero sequence Fourier coefficients are non-existence as it is evident from Figures 10(a) to 10(c), negative sequence coefficients are present due to the negative sequence current. At the phase level, baseband harmonics have the same positions as the case of the balanced load, yet values are higher due to the existence of the negative sequence current and it is conjugated as shown in Figure 10(d). Carrier and sidebands sectors for this type of load show a change in magnitude for the current amplitudes as

depicted in Figures 10(e) and 10(f). The analysis for negative sequence coefficients of the reference phase follows the same route as for the unbalanced load conditions.

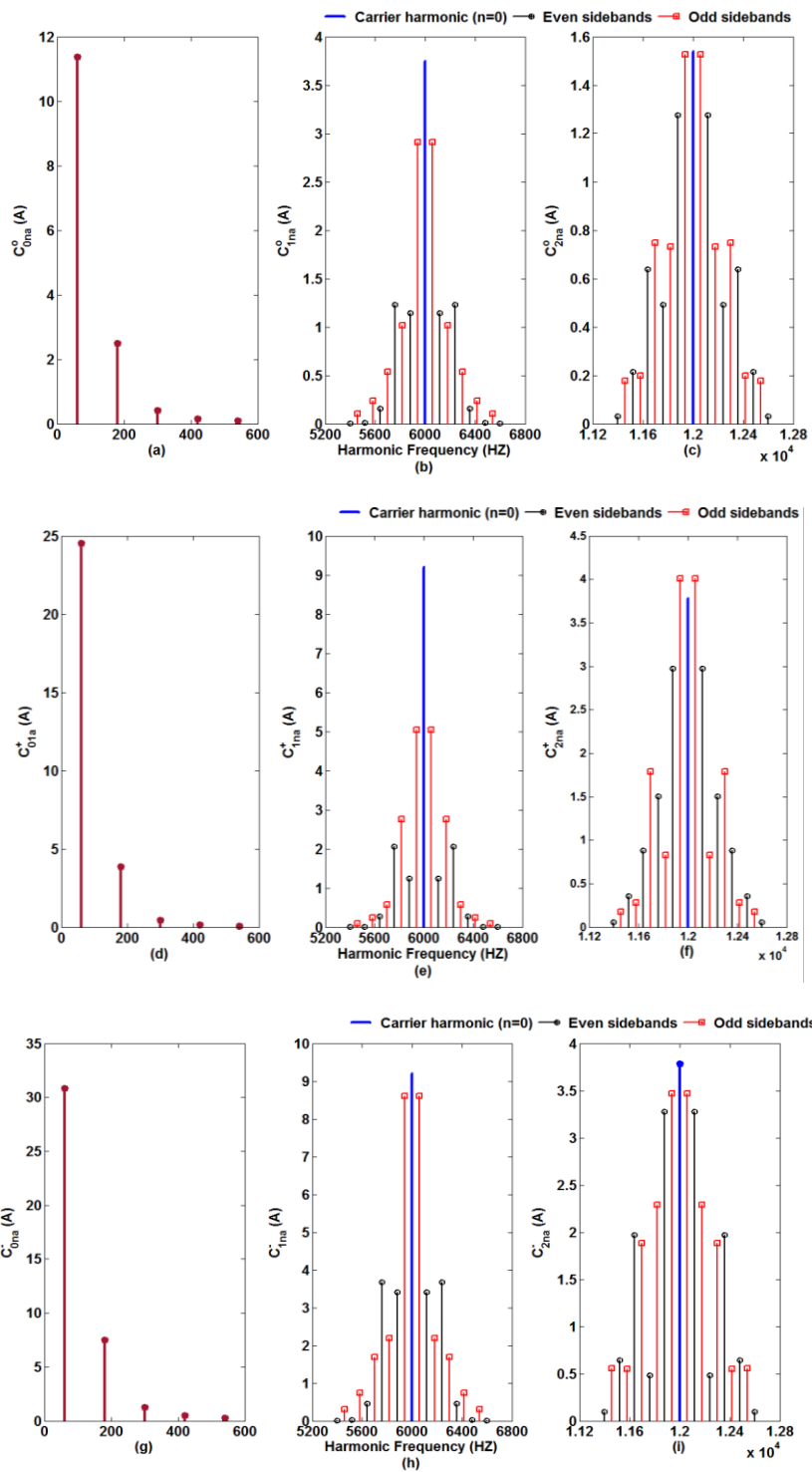


Figure 7. Spectrum per sequence current of phase a for unbalanced/grounded load, (a) baseband sector for zero sequence, (b) carrier and sidebands sector for zero sequence, $m=1$, (c) carrier and sidebands sector for zero sequence, $m=2$, (d) baseband sector for positive sequence, (e) carrier and sidebands sector for positive sequence, $m=1$, (f) carrier and sidebands sector for positive sequence, $m=2$, (g) baseband sector for negative sequence, (h) carrier and sidebands sector for negative sequence, $m=1$, and (i) carrier and sidebands sector for negative sequence, $m=2$

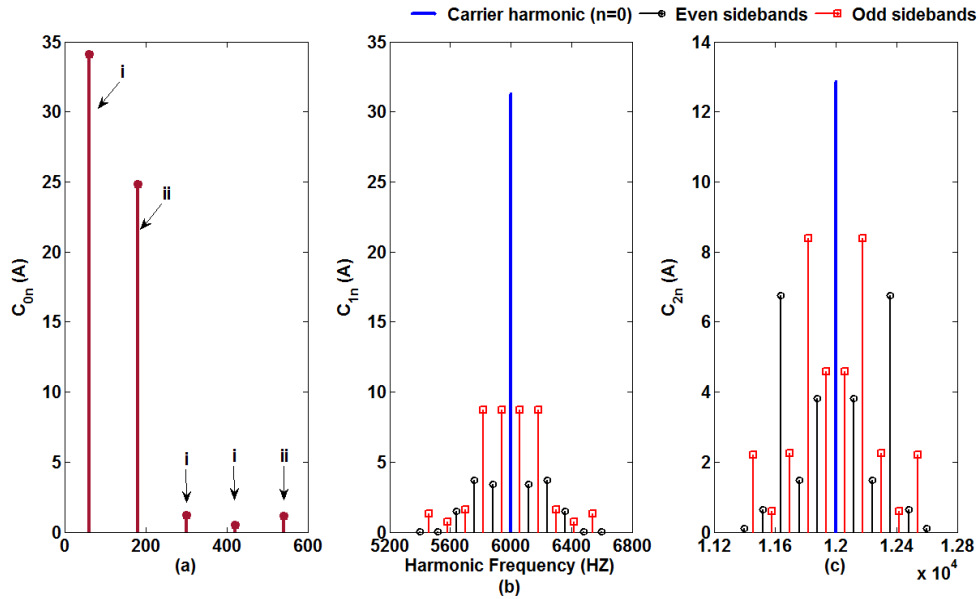


Figure 8. Spectrum of capacitor current based on combined sequence spectrum for unbalanced/grounded load, (a) base band, (b) carrier and sidebands at $m=1$, and (c) carrier and sidebands at $m=2$

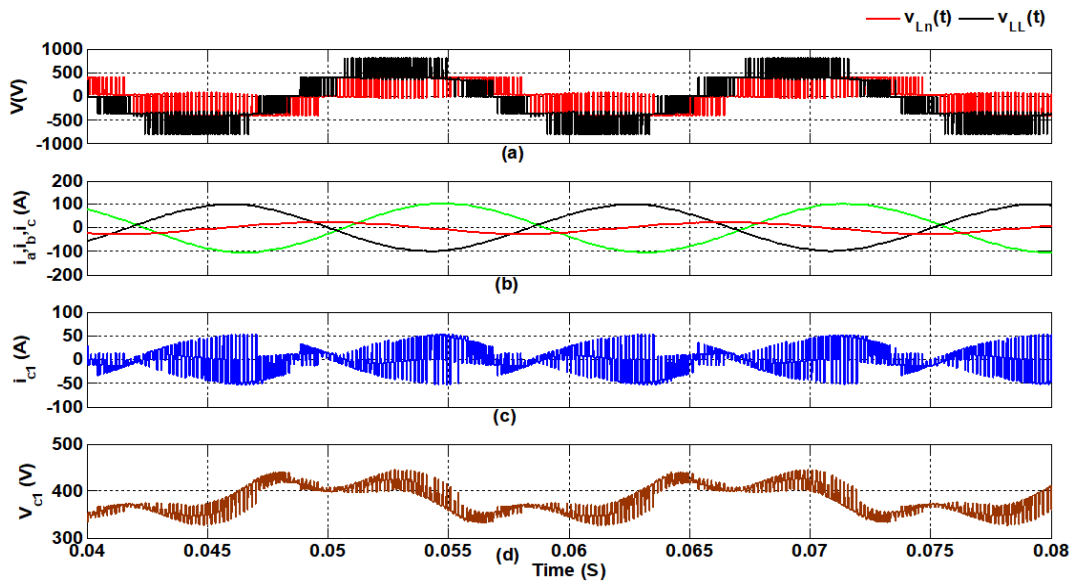


Figure 9. NPC voltage and current for unbalanced/ungrounded load, (a) phase and line-line output voltage, (b) load currents, (c) upper capacitor current, and (d) capacitor voltage

Figure 11 shows the capacitor current spectrum for this case. The main difference from the unbalanced/grounded load condition, is that all amplitudes that are of zero sequence nature are nullified. For example, at the baseband, $C_{01} = 3C_{01a}^o$ is now zero since, $C_{01a}^o = 0$. Amplitudes that are non-zero sequence are still present such as, C_{03} and C_{09} , which are marked by i in Figure 11(a), but of relatively high magnitude as the result of the vector sum of $3C_{03a}^+$ and $3C_{03a}^-$, $3C_{09a}^+$ and $3C_{09a}^-$. Moving on to the carrier and sidebands sector, it is evident from Figure 11(b) that all zero sequence sidebands, odd or even are nullified in the capacitor current for this kind of loading, leaving only sidebands that are function of both positive and negative sequences only. Naturally, the same behavior is encountered for the sector of, $m=2$, as shown in Figure 11(c). The spectrum developed for this type of load is less dense as far as the harmonic content is concerned. Comparing this case with that of unbalanced grounded load, the rms current for the capacitor is less due to the nullified harmonics.

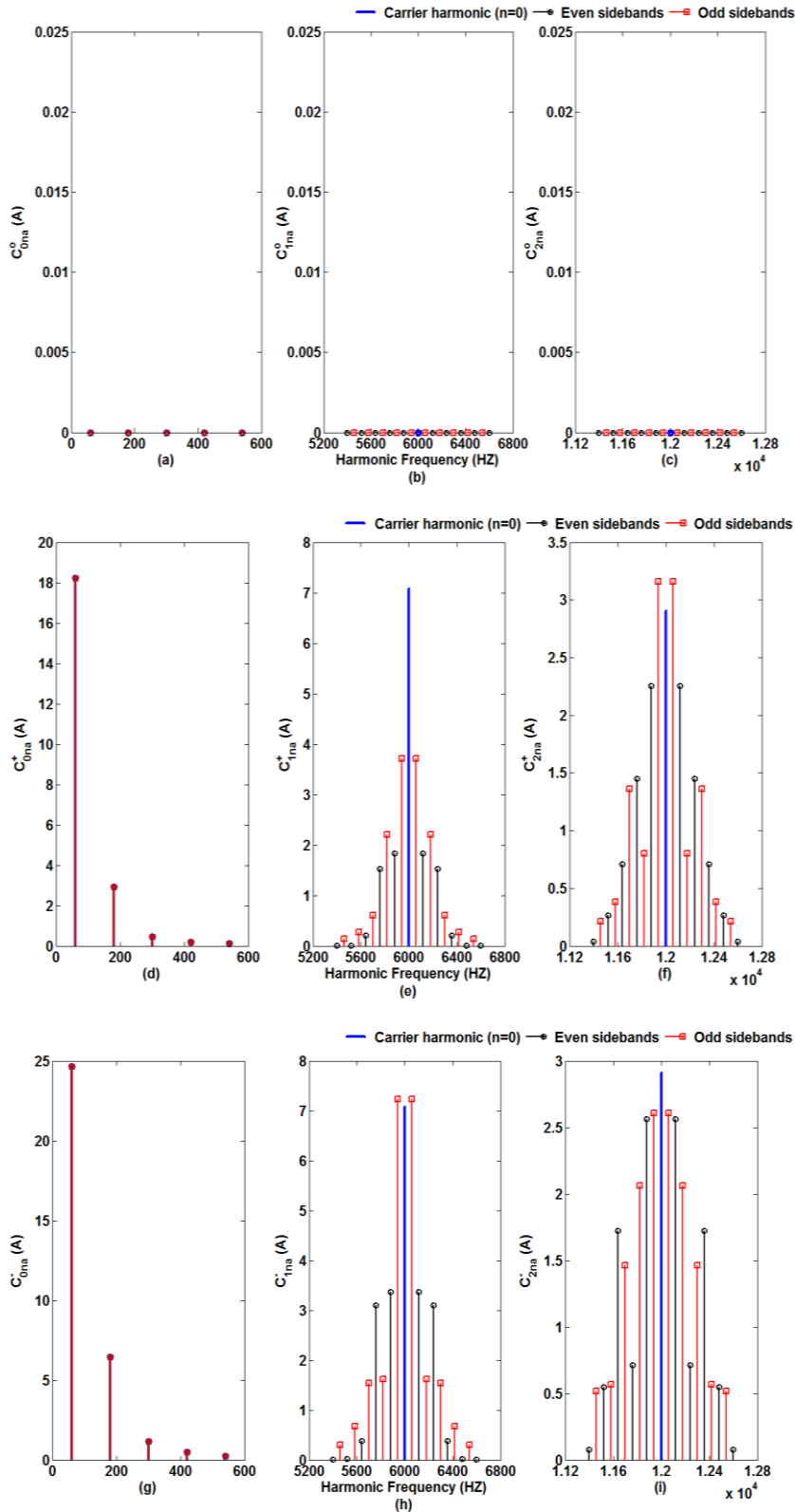


Figure 10. Spectrum per sequence current of phase a for unbalanced/ungrounded load, (a) baseband sector for zero sequence, (b) carrier and sidebands sector for zero sequence, $m=1$, (c) carrier and sidebands sector for zero sequence, $m=2$, (d) baseband sector for positive sequence, (e) carrier and sidebands sector for positive sequence, $m=1$, (f) carrier and sidebands sector for positive sequence, $m=2$, (g) baseband sector for negative sequence, (h) carrier and sidebands sector for negative sequence, $m=1$, and (i) carrier and sidebands sector for negative sequence, $m=2$

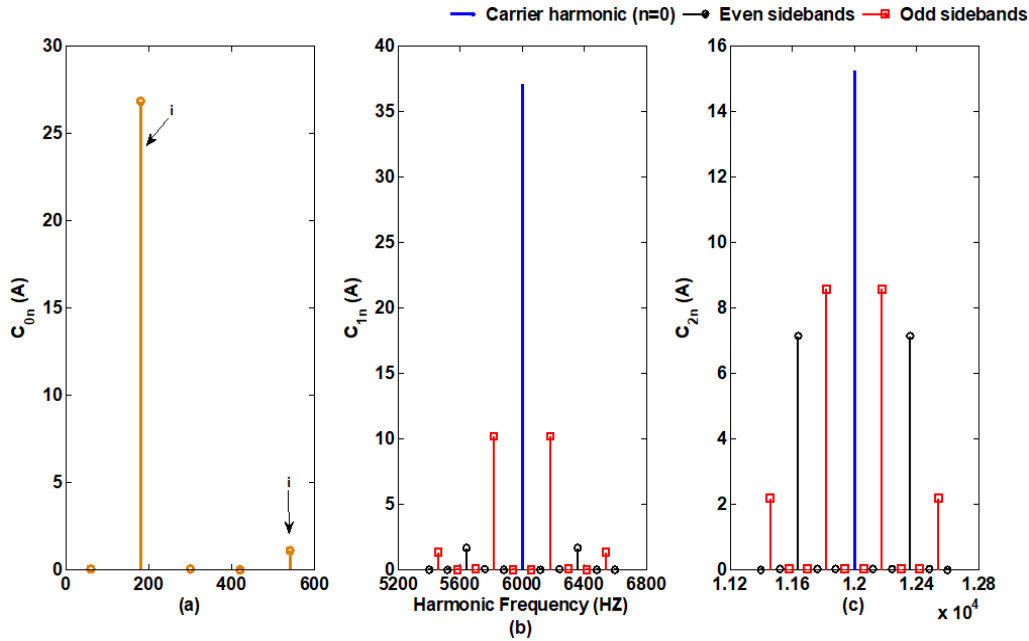


Figure 11. Spectrum of capacitor current based on combined sequence spectrum for unbalanced/ungrounded load, (a) base band, (b) carrier and sidebands at $m=1$, and (c) carrier and sidebands at $m=2$

3.4. Capacitor current formula and voltage ripple analysis

Based on the above simulation results, it is a trivial process to find the NPC capacitor current for each loading condition. The formula for capacitor current is based on the coefficients of the two dimensional Fourier series [28] found for each loading condition. Formulas in this section are presented considering $m = 1.2$ for carrier wave and $n = 1:9$ harmonics for the low frequency wave of the PWM. From the spectrum of Figure 4, the capacitor current formula, for balanced load is,

$$i_{C1-\frac{Bal}{Gr}} = 24.3179e^{j(3\omega_0 t + 40.893^\circ)} + 1.1077e^{j(9\omega_0 t - 111.05^\circ)} + 30.678e^{j(\omega_c t + 180^\circ)} + 12.604e^{j(2\omega_c t)} + 8.546e^{j(3\omega_0 t + \omega_c t + 163.661^\circ)} + 1.303e^{j(9\omega_0 t + \omega_c t + 163.661^\circ)} + 8.224e^{j(3\omega_0 t + 2\omega_c t - 125.538^\circ)} + 2.151e^{j(9\omega_0 t + 2\omega_c t - 118.798^\circ)} + 1.442e^{j(6\omega_0 t + \omega_c t + 32.645^\circ)} + 6.617e^{j(6\omega_0 t + 2\omega_c t + 46.634^\circ)}$$

Hence, for balanced loads fed by the NPC, the AC ripples in the capacitor current are composed from baseband, carrier harmonics and sidebands of odd order and one even sideband at $n=6$. The current i_{C1} , for the unbalanced/grounded load, is found from the simulation results of section 3.2,

$$i_{C1-Unbal/Gr} = 34.108e^{j(\omega_0 t + 171.1243^\circ)} + 24.818e^{j(3\omega_0 t + 40.893^\circ)} + 1.221e^{j(5\omega_0 t - 37.983^\circ)} + 0.4754e^{j(7\omega_0 t + 132.452^\circ)} + 1.13e^{j(9\omega_0 t - 111.052^\circ)} + 31.309e^{j(\omega_c t + 180^\circ)} + 12.8635e^{j(2\omega_c t)} + 8.738e^{j(\omega_0 t + \omega_c t + 159.761^\circ)} + 8.722e^{j(3\omega_0 t + \omega_c t + 163.661^\circ)} + 1.303e^{j(5\omega_0 t + \omega_c t - 39.194^\circ)} + 0.709e^{j(7\omega_0 t + \omega_c t + 139.104^\circ)} + 1.329e^{j(9\omega_0 t + \omega_c t - 114.037^\circ)} + 4.582e^{j(\omega_0 t + 2\omega_c t + 5.638^\circ)} + 8.393e^{j(3\omega_0 t + 2\omega_c t - 125.538^\circ)} + 2.242e^{j(5\omega_0 t + 2\omega_c t + 177.961^\circ)} + 0.5927e^{j(7\omega_0 t + 2\omega_c t + 110.1963^\circ)} + 2.195e^{j(9\omega_0 t + 2\omega_c t - 118.799^\circ)} + 3.437e^{j(2\omega_0 t + \omega_c t - 31.52^\circ)} + 3.691e^{j(4\omega_0 t + \omega_c t - 21.693^\circ)} + 1.471e^{j(6\omega_0 t + \omega_c t + 32.6455^\circ)} + 0.0249e^{j(8\omega_0 t + \omega_c t - 18.321^\circ)} + 3.8264e^{j(2\omega_0 t + 2\omega_c t - 3.754^\circ)} + 1.478e^{j(4\omega_0 t + 2\omega_c t - 125.198^\circ)} + 6.753e^{j(6\omega_0 t + 2\omega_c t + 46.634^\circ)} + 0.646e^{j(8\omega_0 t + 2\omega_c t - 46.634^\circ)}$$

The unbalanced/ungrounded load condition results in a capacitor current which is expressed based on the frequency spectrum coefficients of section 3.3 as,

$$\begin{aligned}
i_{C1-Unbal/Ungr} = & 26.3844e^{j(3\omega_0t+34.071^\circ)} + 1.088e^{j(9\omega_0t-116.237^\circ)} + 37.11e^{j(\omega_ct+180^\circ)} \\
& + 15.246e^{j(2\omega_ct)} + 10.177e^{j(3\omega_0t+\omega_ct+167.105^\circ)} + 1.294e^{j(9\omega_0t+\omega_ct-119.73^\circ)} \\
& + 8.568e^{j(3\omega_0t+2\omega_ct-132.448^\circ)} + 2.177e^{j(9\omega_0t+2\omega_ct-125.142^\circ)} \\
& + 1.6424e^{j(6\omega_0t+\omega_ct+26.579^\circ)} + 7.132e^{j(6\omega_0t+2\omega_ct+39.584^\circ)}
\end{aligned}$$

Based on the above capacitor current expressions for each loading condition, the rms capacitor current can be calculated and is shown in Table 2. The unbalanced grounded load has the highest rms ripple current and this is attributed to the number of ripple components compared to the balanced and unbalanced/ungrounded loadings. In the case where no ground path exists, many of the zero sequence ripple components are of zero value, hence a decrease in the rms capacitor component is obtained. Capacitor voltage ripples can also be evaluated for each case. Voltage ripple in this work is estimated as the peak deviation of the NPC capacitor voltage from the nominal DC voltage [30]. Percentage voltage ripples are also shown in Table 2, where Vr_{C1} is the percentage voltage ripple of the upper capacitor. It is clear that as the load deviates from balanced conditions, the voltage ripple increases which may result in significant distortion of the converter output voltage. At balanced conditions, the capacitor voltage deviation is at 10.303% which may be tolerated in practical applications. However, for an unbalanced/grounded load, the deviation jumps to 22.673% which needs a change in capacitor to decrease the value to a tolerated level. Hence, the analyses presented in this work can be employed as a systematic method to evaluate and cure capacitor voltage ripples. In that context, the required capacitor value can be easily determined, using the two-dimensional Fourier expansion, for a specific load condition with unbalanced characteristics.

Table 2. Capacitor current and percentage voltage ripple for loads under study

Capacitor current/percentage voltage ripple	Value
$i_{C1-Bal/Gr}$	30.704 A
$i_{C1-Unbal/Gr}$	40.478 A
$i_{C1-Unbal/Ungr}$	35.836 A
$Vr_{C1-Bal/Gr}$	10.303%
$Vr_{C1-Unbal/Gr}$	22.673%
$Vr_{C1-Unbal/Ungr}$	12.736%

4. CONCLUSION

The load on the 3L-NPC can become unbalanced due to any random effects such as one phase switch off or asymmetrical currents in terms of magnitude, phase or both. Therefore, analyzing of the capacitor current is a demanding need. One means of analysis is to investigate the harmonic spectrum of the capacitor current under unbalanced loading effects. It is shown in this work that the two-dimensional Fourier method with symmetrical components decomposition provides a powerful mean to derive the required spectrum and document the harmonics content in the converters' capacitor current. Results in this paper verify that the spectrum is not only a function of whether the load is balanced or not but also depends on the existence of ground path which adds zero sequence harmonics in all sectors of the spectrum. The latter affects both the rms current of the capacitor and voltage ripples. Analysis proposed in this paper documents that an unbalanced load with a ground path considerably changes the harmonic spectrum which calls for capacitor value variation in order to achieve a tolerated voltage ripple.

REFERENCES

- [1] A. Nabae, I. Takahashi, and H. Akagi, "A new neutral-point-clamped PWM inverter," *IEEE Transactions on Industry Applications*, vol. IA-17, no. 5, pp. 518–523, Sep. 1981, doi: 10.1109/TIA.1981.4503992.
- [2] R. Teichmann and S. Bernet, "A comparison of three-level converters versus two-level converters for low-voltage drives, traction, and utility applications," *IEEE Transactions on Industry Applications*, vol. 41, no. 3, pp. 855–865, May 2005, doi: 10.1109/TIA.2005.847285.
- [3] A. Choudhury, P. Pillay, and S. S. Williamson, "Comparative analysis between two-level and three-level DC/AC electric vehicle traction inverters using a novel DC-link voltage balancing algorithm," *IEEE Journal of Emerging and Selected Topics in Power Electronics*, vol. 2, no. 3, pp. 529–540, Sep. 2014, doi: 10.1109/JESTPE.2014.2310140.
- [4] J. Rodriguez, J.-S. Lai, and F. Z. Peng, "Multilevel inverters: a survey of topologies, controls, and applications," *IEEE Transactions on Industrial Electronics*, vol. 49, no. 4, pp. 724–738, Aug. 2002, doi: 10.1109/TIE.2002.801052.
- [5] L. Jih-Sheng and Z. P. Fang, "Multilevel converters-a new breed of power converters," *IEEE Transactions on Industry Applications*, vol. 32, no. 3, pp. 509–517, 1996, doi: 10.1109/28.502161.
- [6] H.-P. Krug, T. Kume, and M. Swamy, "Neutral-point clamped three-level general purpose inverter-features, benefits and applications," in *2004 IEEE 35th Annual Power Electronics Specialists Conference (IEEE Cat. No.04CH37551)*, 2004, pp. 323–328, doi: 10.1109/PESC.2004.1355764.
- [7] S. Kouro *et al.*, "Recent advances and industrial applications of multilevel converters," *IEEE Transactions on Industrial*

- Electronics*, vol. 57, no. 8, pp. 2553–2580, Aug. 2010, doi: 10.1109/TIE.2010.2049719.
- [8] Y. Wang and F. Wang, "Novel three-phase three-level-stacked neutral point clamped grid-tied solar inverter with a split phase controller," *IEEE Transactions on Power Electronics*, vol. 28, no. 6, pp. 2856–2866, Jun. 2013, doi: 10.1109/TPEL.2012.2226475.
 - [9] M. Benadja and A. Chandra, "Adaptive sensorless control of PMSGs-based offshore wind farm and VSC-HVdc stations," *IEEE Journal of Emerging and Selected Topics in Power Electronics*, vol. 3, no. 4, pp. 918–931, Dec. 2015, doi: 10.1109/JESTPE.2015.2453113.
 - [10] A. M. Razali, N. A. Yusoff, K. A. Karim, A. Jidin, and T. Sutikno, "A new switching look-up table for direct power control of grid connected 3L-NPC PWM rectifier," *International Journal of Power Electronics and Drive Systems (IJPEDS)*, vol. 12, no. 3, pp. 1413–1421, Sep. 2021, doi: 10.11591/ijpeds.v12.i3.pp1413-1421.
 - [11] A. A. Abbood, "Harmonic spectra of BLDC motor supplied by a solar PV multilevel inverter," *Indonesian Journal of Electrical Engineering and Computer Science (IJECS)*, vol. 20, no. 3, Dec. 2020, doi: 10.11591/ijeecs.v20.i3.pp1693-1702.
 - [12] A. A. Abdelsalam, M. A. Esmaeel, and S. A. Zaid, "Two-level inverter and three-level neutral point diode clamped inverter for traction applications: a comparative analysis study," *International Journal of Power Electronics and Drive Systems (IJPEDS)*, vol. 12, no. 3, pp. 1609–1619, Sep. 2021, doi: 10.11591/ijpeds.v12.i3.pp1609-1619.
 - [13] G. Dyanamina and S. K. Kakodia, "Adaptive neuro fuzzy inference system based decoupled control for neutral point clamped multi level inverter fed induction motor drive," *Chinese Journal of Electrical Engineering*, vol. 7, no. 2, pp. 70–82, Jun. 2021, doi: 10.23919/CJEE.2021.000017.
 - [14] J. Rodriguez, S. Bernet, P. K. Steimer, and I. E. Lizama, "A survey on neutral-point-clamped inverters," *IEEE Transactions on Industrial Electronics*, vol. 57, no. 7, pp. 2219–2230, Jul. 2010, doi: 10.1109/TIE.2009.2032430.
 - [15] S. Bo, L. Xinyi, L. Wanting, Z. Hui, and L. Ning, "A new carrier based neutral point potential control strategy for three-level NPC converter," in *2018 IEEE 4th Information Technology and Mechatronics Engineering Conference (ITOEC)*, Dec. 2018, pp. 427–431, doi: 10.1109/ITOEC.2018.8740588.
 - [16] A. Videt, P. Le Moigne, N. Idir, P. Baudesson, and J. Ecrabey, "A new carrier-based PWM for the reduction of common mode currents applied to neutral-point-clamped inverters," in *APEC 07-Twenty-Second Annual IEEE Applied Power Electronics Conference and Exposition*, Feb. 2007, pp. 1224–1230, doi: 10.1109/APEX.2007.357671.
 - [17] L. M. A. Alsaqa, A. M. T. I. Alnaib, and O. T. Mahmood, "Comparison of multiple modulation techniques for various topologies of multilevel converters for single phase AC motor drive," *International Journal of Power Electronics and Drive Systems (IJPEDS)*, vol. 10, no. 2, pp. 662–671, Jun. 2019, doi: 10.11591/ijpeds.v10.i2.pp662-671.
 - [18] Z. M. Tahir, A. Jidin, and M. L. M. Jamil, "Multi-carrier switching strategy for high-bandwidth potential balancing control of multilevel inverters," *International Journal of Power Electronics and Drive Systems (IJPEDS)*, vol. 12, no. 4, pp. 2384–2392, Dec. 2021, doi: 10.11591/ijpeds.v12.i4.pp2384-2392.
 - [19] J. Wang, Y. Gao, and W. Jiang, "A carrier-based implementation of virtual space vector modulation for neutral-point-clamped three-level inverter," *IEEE Transactions on Industrial Electronics*, vol. 64, no. 12, pp. 9580–9586, Dec. 2017, doi: 10.1109/TIE.2017.2711550.
 - [20] P. Kiatsookkanatorn and N. Watjanatepin, "Novel ripple reduction method using three-level inverters with unipolar PWM," *Indonesian Journal of Electrical Engineering and Computer Science (IJECS)*, vol. 22, no. 3, pp. 1272–1283, Jun. 2021, doi: 10.11591/ijeecs.v22.i3.pp1272-1283.
 - [21] M. Wu, C. Xue, Y. W. Li, and K. Yang, "A generalized selective harmonic elimination PWM formulation with common-mode voltage reduction ability for multilevel converters," *IEEE Transactions on Power Electronics*, vol. 36, no. 9, pp. 10753–10765, Sep. 2021, doi: 10.1109/TPEL.2021.3063299.
 - [22] R. M. Tallam, R. Naik, and T. A. Nondahl, "A carrier-based PWM scheme for neutral-point voltage balancing in three-level inverters," *IEEE Transactions on Industry Applications*, vol. 41, no. 6, pp. 1734–1743, Nov. 2005, doi: 10.1109/TIA.2005.858283.
 - [23] F. Chen, W. Qiao, H. Wang, and L. Qu, "A simple zero-sequence voltage injection method for carrier-based pulsewidth modulation of the three-level NPC inverter," *IEEE Journal of Emerging and Selected Topics in Power Electronics*, vol. 9, no. 4, pp. 4687–4699, Aug. 2021, doi: 10.1109/JESTPE.2020.3012726.
 - [24] D. N. Quy, D. Ba Phu, and N. K. Trung, "The new approach minimizes harmonics in a single-phase three-level NPC 400 Hz converter for airplanes," *International Journal of Power Electronics and Drive Systems (IJPEDS)*, vol. 12, no. 3, pp. 1738–1750, Sep. 2021, doi: 10.11591/ijpeds.v12.i3.pp1738-1750.
 - [25] Z. Ye, Y. Xu, X. Wu, G. Tan, X. Deng, and Z. Wang, "A simplified PWM strategy for a neutral-point-clamped (NPC) three-level converter with unbalanced DC links," *IEEE Transactions on Power Electronics*, vol. 31, no. 4, pp. 3227–3238, Apr. 2016, doi: 10.1109/TPEL.2015.2446501.
 - [26] X. Wu, G. Tan, G. Yao, C. Sun, and G. Liu, "A hybrid PWM strategy for three-level inverter with unbalanced DC links," *IEEE Journal of Emerging and Selected Topics in Power Electronics*, vol. 6, no. 1, pp. 1–15, Mar. 2018, doi: 10.1109/JESTPE.2017.2756999.
 - [27] S. R. Pulikanti, M. S. A. Dahidah, and V. G. Agelidis, "Voltage balancing control of three-level active NPC converter using SHE-PWM," *IEEE Transactions on Power Delivery*, vol. 26, no. 1, pp. 258–267, Jan. 2011, doi: 10.1109/TPWRD.2010.2063718.
 - [28] D. G. Holmes and T. A. Lipo, *Pulse width modulation for power converters*. IEEE, 2003.
 - [29] S. S. Thakur, M. Odavic, A. Allu, Z. Q. Zhu, and K. Atallah, "Theoretical harmonic spectra of PWM waveforms including DC bus voltage ripple-application to a low-capacitance modular multilevel converter," *IEEE Transactions on Power Electronics*, vol. 35, no. 9, pp. 9291–9305, Sep. 2020, doi: 10.1109/TPEL.2020.2974156.
 - [30] G. I. Orfanoudakis, "Analysis and reduction of dc-link capacitor voltage/current stress in three-level PWM converters," University of Southampton, 2012.
 - [31] G. C. Paap, "Symmetrical components in the time domain and their application to power network calculations," *IEEE Transactions on Power Systems*, vol. 15, no. 2, pp. 522–528, May 2000, doi: 10.1109/59.867135.
 - [32] J. D. Glover, M. S. Sarma, and T. J. Overbye, *Power system analysis and design*, Fifth edit. Cengage Learning, 2008.
 - [33] A. Poularikas, *The handbook of formulas and tables for signal processing*. Boca Raton: CRC Press LLC, 1999.

BIOGRAPHIES OF AUTHORS

Riyadh Toman Thahab    obtained his B.Sc. in Electrical Engineering from the University of Babylon in 1998. He was admitted to the graduate program in the University of Technology in Baghdad where he graduated with an M.Sc. degree in electric power systems. He joined the doctoral program at the College of Engineering and Applied Sciences, Western Michigan University, USA, in 2012 and graduated in December 2017. Currently he is an Associate Professor in the Department of Electrical Engineering at the University of Babylon, College of Engineering. His research interests include power electronics converters, integration of renewable energy sources, multilevel converters and control of power converters for microgrid applications. He can be contacted at email: riyadhtomanth.toman@wmich.edu.



Tahani Hamodi Al-Mhana    received the B.Sc. degree from Mosul University, Mosul, Iraq, in 1992, and the M.Sc. degree from University of Technology, Baghdad, Iraq, in 2000, both in electrical engineering/power engineering, and the Ph.D. degree in electrical and electronic engineering from Newcastle University, Newcastle upon Tyne, U.K., in 2016. Since 1992, she has been with the Department of Electrical Engineering, University of Babylon, Iraq, where she is currently an Associate Professor in Electrical Engineering. Her current research interests include power electronics converters for transport applications, renewable energy integration, power system compensation, and machine control. She can be contacted at email: eng.tahany.hamodi@uobabylon.edu.iq.



Ahmed Toman Thahab    is an Associate Professor at the University of Babylon. He received his B.Sc. in Electrical Engineering in 2006. He also holds a M.Sc. in communication engineering since 2011. Currently he is an Associate Professor at the University of Babylon, Department of Biomedical Engineering. He can be contacted at email: eng.ahmed.t.thahab@uobabylon.edu.iq.